Emptying-filling boxes with non-Boussinesq plumes and fountains

R. Mehaddi ⬤[*] and P. Boulet
LEMTA, CNRS, Université de Lorraine, 54000 Nancy, France

M. Koutaiba
Centre Scientifique et Technique du Bâtiment, Université Paris-Est, 77420 Champs-sur-Marne, France

O. Vauquelin⬤ and F. Candelier⬤
IUSTI, UMR No. 7343, CNRS, Université d'Aix-Marseille, 13013 Marseille, France

In this paper the dynamics of the simultaneously filling and emptying of a box is studied theoretically and experimentally. Both situations, consisting of negatively buoyant (fountains) and positively buoyant (plumes) discharges, are considered. For the sake of generality, no assumption is made about the value of the density deficit (between the release and the ambient fluid), so this study deals with the so-called non-Boussinesq general case. Experiments are carried out with buoyant air-helium mixtures continuously released from the top (fountain) or bottom (plume) into air in a cylindrical tank with an open bottom boundary and a top vent of variable areas. At steady state, for both fountain and plume configurations, a buoyant layer of constant thickness and density forms under the tank ceiling. Based on mass and buoyancy conservation equations applied on the buoyant layer, theoretical models are proposed to estimate its depth and density at steady state. The theoretical models compare favorably with the experimental data. Subsequently, these models allow us to compare the plume and the fountain configurations for identical source conditions, box size, and vent area. Even if, in the majority of situations, the plume configuration allows a better mixing of the buoyant fluid with the environment, it is found that beyond a certain value of the fountain height, the fountain configuration becomes more efficient than the plume configuration for mixing phenomena.

I. INTRODUCTION

The continuous release of a buoyant fluid into confined and semiconfined environments is a widespread phenomenon in nature and industry such as building natural ventilation [1], chemical processes [2], and geophysical flows [3,4], to name but a few. In all these applications, the buoyant fluid can be injected in the form of either a plume (positively buoyant release [5]) or a fountain (negatively buoyant release [6,7]). Thus, in a box, the release of a fluid lighter than the ambient fluid will give rise to a plume in the case of an upward injection (from the bottom) or a fountain in the case of a downward injection (from the ceiling). The aim of the present study is to compare, for the same release, both configurations in the particular case where the enclosure has a vent area at its ceiling. These two situations correspond to the so-called emptying-filling box problem.

In the plume case, a layer of buoyant fluid forms under the box ceiling and grows with time due to the volume flux delivered by the plume. At the same time, a part of this fluid escapes

---

[*]rabah.mehaddi@univ-lorraine.fr

through the vent located at the ceiling owing to the density difference between the buoyant layer and the outer fluid. After a while, the fluid layer thickness stabilizes and the fluid density eventually stabilizes around constant values, thus defining the steady-state regime. The simultaneous filling and emptying of an enclosure was first analyzed both theoretically and experimentally by Linden *et al.* [8], under the Boussinesq assumption (i.e., for small density differences). Using the conservation equations of volume and buoyancy for the buoyant layer, these authors obtained analytically the layer thickness as well as its density. A striking result is that, at steady state, the layer thickness only depends on the ratio between the vent area and the square of the enclosure height. The case of a large density difference between the plume and the ambient (i.e., the non-Boussinesq case) was studied by Vauquelin [9]. In that case, an additional parameter appears. This parameter accounts for the influence of the source buoyancy flux. However, the weaknesses of these two theoretical studies lie in the modeling of the plume. These studies are indeed both based on the far-field self-similar solutions of the plume originally introduced by Morton and Turner [5,10]. These solutions correspond to a plume issuing from a point source of buoyancy without source mass and momentum fluxes. However, this model is not realistic for a real plume which has a source of finite size. To represent the plume variables without singularities, an alternative model, based on the so-called plume function, was proposed among others by Morton [5] and Hunt and Kaye [11] for Boussinesq plumes and by Michaux and Vauquelin [12] and Candelier and Vauquelin [13] for non-Boussinesq plumes. In this study we propose to revisit the emptying-filling box problem by using these analytical developments on turbulent non-Boussinesq plumes.

Unlike the case of plumes, much less attention has been directed to the topic of fountains developing in confined environments. Among the few authors interested in fountains in confined and semiconfined environments, we can cite the work by Baines *et al.* [14]. These authors studied the filling of a box with a fountain, both theoretically and experimentally. To produce fountains, the authors injected from below salt water into a tank initially filled up with fresh water. The fountain rises initially as a jet due to the source momentum of the release but slows down gradually owing to its negative buoyancy. Thus, the fountain reaches a finite height before collapsing under the form of an annular downflow surrounding an inner upflow. When this downflow reaches the floor, a negatively buoyant layer of fluid forms, similarly to the plume case. The study by Baines *et al.* [14] mainly focused on determining the time evolution of the buoyant-layer depth and density. In particular, they identified two phases in the filling process.

(i) First, the buoyant-layer depth grows over time due to the fountain source volume flux and to the volume flux of ambient air entrained by the part of the fountain that penetrates vertically beyond the buoyant-layer depth.

(ii) The second phase of replenishment involves only the fountain source volume flux since the buoyant layer has completely submerged the fountain. Then its evolution in time becomes linear, similarly to the filling of a bathtub with a submerged water jet.

As observed by Baines *et al.* [14], in order to accurately determine the growth of the buoyant layer in the first phase, the key parameter is the fountain entrainment coefficient. On the basis of dimensional considerations, these authors found that the ratio between the bulk entrainment flux and the source volume flux is proportional to the height of the fountain extending above the buoyant layer. In the present study, the aim is to extend the model by Baines *et al.* [14] to the simultaneous emptying-filling situation.

In some applications such as thermal comfort of buildings, one may wonder if it is more appropriate to inject hot air downward (fountain) or upward (plume), and vice versa, in the case of air conditioning. Intuitively, one might argue that the plume is the most efficient flow to produce a uniform temperature field into a room. Nevertheless, Baines *et al.* [14] highlighted the important potential of a fountain to entrain strongly its surrounding and then to create mixing. In this case, the comparison of the two modes of injection seems to be relevant to this issue of thermal comfort. In addition, in other applications such as accidental release of heavy or light gases [15] and fires in building [16–18], it would be desirable, sometimes, rather not to mix in order to maintain the natural stratification. Thus, it is also interesting to compare these two injection modes.
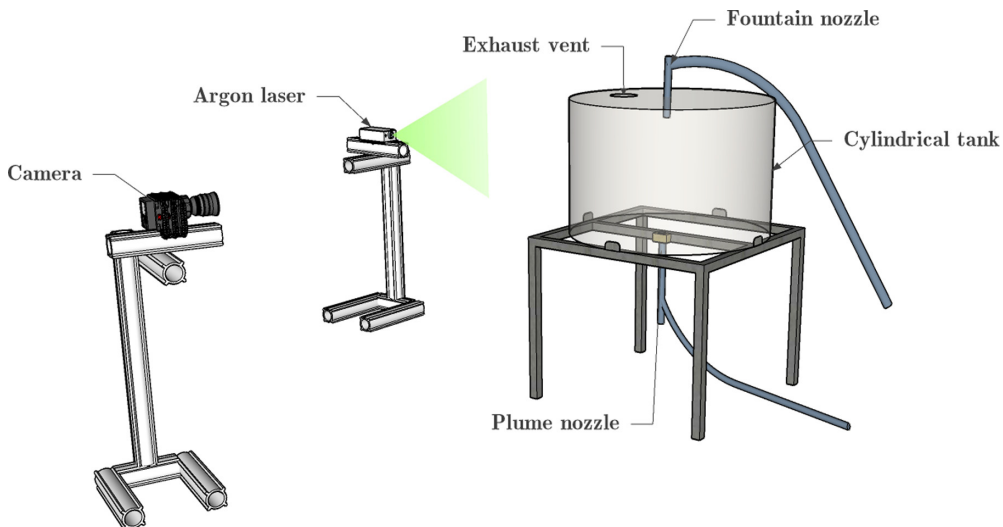
FIG. 1. Schematic of the experimental apparatus.

To answer such questions, we propose in this paper to compare two theoretical models. These models are based on the conservation equations of mass and buoyancy of the buoyant layer. The aim is to take into account both the non-Boussinesq effects and the effects associated with the finite-size source. Since these theoretical models require validation and/or calibration, experiments are carried out with releases of air-helium mixture injected into a cylindrical tank with a vent area at its ceiling. Note that these experiments allow large density contrasts to be reached so that the results turn out to be reliable for thermal comfort applications [19] but also for problems involving large density differences out of the Boussinesq assumption.

The paper is organized as follows. In Sec. II the experimental apparatus is presented. In Sec. III a model is proposed for the simultaneously filling and emptying of the box with a plume. This model is validated against experimental data. In Sec. IV a model for filling and emptying with a fountain is proposed. Similarly to the plume case, the model is compared to experimental data. In Sec. V the plume and fountain theoretical models are compared with identical source conditions, box size, and vent area. A summary is given in Sec. VI.

II. EXPERIMENTS

The experimental apparatus is schematically shown in Fig. 1. It is composed of a cylindrical tank made of plexiglass; its height is 80 cm and its diameter is 120 cm. Similarly to the experiments by Baines *et al.* [14], the bottom of the cylindrical tank is fully open to the atmosphere (i.e., the cylinder constitutes a so-called open chamber). This is an important point for the theory because it will be assumed later that both fountains and plumes are allowed to freely entrain the ambient fluid without any confinement effects. Since our experiments consider the simultaneous filling and emptying box processes, the top surface of the cylinder tank involves a circular opening allowing the buoyant fluid to flow out of the box. The diameter of this opening varies in our experiments.

The turbulent fountains and plumes used to fill the tank are produced by a continuous discharge of an air-helium mixture. In order to accurately control the density of the mixture, air and helium initially flow through independent networks and their respective flow rates are measured with flow meters (Bronkhorst model EL-FLOW, with a relative error of 2%). The two fluids are then mixed and the resulting mixture is made visible with passive tracers before being injected in a cylindrical tank through a nozzle of radius b_i. Two different nozzles have been used with respective radii of 3 and 6 mm. Note that the passive tracer is ammonium salt. It is obtained by a chemical reaction of

TABLE I. Details of the experimental parameters for the plume case.

Configuration	b_i (mm)	u_i (m/s)	ρ_i (kg/m^3)	η_i	H (mm)	Γ_i	Re
1	3	17.68	0.69	0.43	665	2.8×10^{-4}	1955
2	6	7.95	1.025	0.16	600	8.4×10^{-4}	2600
3	6	24.16	0.31	0.75	600	7.8×10^{-4}	2400

ammonia vapor with hydrochloric acid [20,21]. The mass of salt added to the flow is very weak and therefore does not affect the density of the fountain.

To visualize the flow, a laser sheet produced by a 2-W argon laser is used. The laser sheet cuts the cylindrical box at its center in order to visualize the flow development as well as the formation of the buoyant layer. Images are recorded by a high-speed camera (PCO 1200hs) and are postprocessed using MATLAB software in order to determine the location of the interface between the buoyant fluid and the ambient.

Usually, the control parameters of the release are the source plume function Γ_i, the source Reynolds number Re, and the density deficit η_i which accounts for the non-Boussinesq effects. These parameters are defined, respectively, as

$$\Gamma_i = \frac{5gb_i\eta_i}{8\alpha\sqrt{1-\eta_i}u_i^2}, \quad \mathrm{Re} = \frac{\rho_i u_i b_i}{\mu}, \quad \eta_i = \frac{\Delta\rho}{\rho_a}, \tag{1}$$

where u_i is the bulk velocity at the source, $\Delta\rho = \rho_a - \rho_i$ is the density difference between the ambient (subscript a) and the source fluid (subscript i), g is the gravitational acceleration, and α is the plume entrainment coefficient introduced by Morton and Turner [10]. Note that the source plume function Γ_i is equivalent to the Richardson number. It quantifies the importance of the buoyancy with respect to the momentum at the source. When $\Gamma_i < 1$, the released fluid is dominated by its momentum and then the plume is referred to as a forced plume, while when $\Gamma_i > 1$, the plume is dominated by its buoyancy and called a lazy plume. The case $\Gamma_i = 1$ corresponds to a pure plume.

To measure the effects of the exhaust vent, we introduce the parameter

$$\Sigma = \frac{4\sqrt{\alpha}C_d A}{\sqrt{5}\pi b_i^2}, \tag{2}$$

where C_d is a discharge coefficient accounting for streamline contraction. Its value lies between 0.6 and 0.7 and is generally constant for high Reynolds number [22]. References [23,24] show that this coefficient is a function of the layer depth and its density contrast. This effect is important in the transient phase and becomes negligible as soon as the layer reaches its steady state. In what follows, we choose the value $C_d = 0.7$, which seems very common in natural ventilation problems [25,26].

For plume releases, three configurations are considered. For each configuration, the source conditions (Re, Γ_i, and η_i) and the distance between the source and the ceiling (denoted by H) are kept fixed while the vent area is varied (see Table I). Seven circular vent areas are considered with respective diameters of 50, 80, 100, 120, 150, 170, and 200 mm and one square vent area with a size of 200 × 200 mm^2. These configurations correspond to 24 experiments. A visualization of the flow pattern is shown in Fig. 2(a).

In the case of fountain releases, 34 experiments are carried out. In these experiments, the source density deficit $\eta_i = \Delta\rho/\rho_a$ is varied in the range $0.86 > \eta_i > 0.28$ and the parameter Γ_i is varied in the range 0.0015–0.043. The fountain source Reynolds number Re is varied in the range $655 <$ Re < 2160. Note that the radius $b_i = 7$ mm is kept constant for all the fountain experiments. An illustration of a typical experiment is shown in Fig. 2(b). When the steady state is reached, there are two possibilities: The fountain is fully submerged by the buoyant layer or the fountain is only partially submerged by the buoyant layer. In the first case, the air-entrainment process induced by the fountain vanishes and therefore the volume flow rate at the outlet opening balances that injected into the tank from the source. In the second case, the fountain is only partially submerged, so the
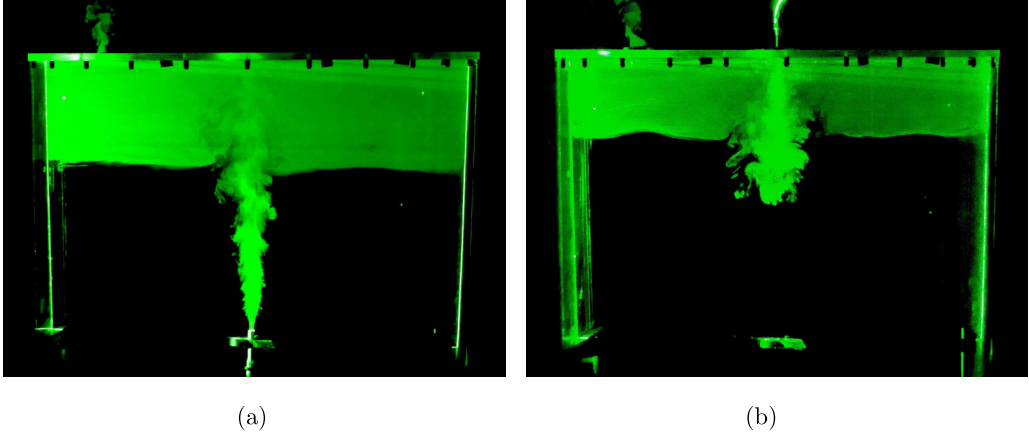
(a)

(b)

FIG. 2. Illustration of (a) plume and (b) fountain filling-emptying box experiments.

volume flow rate at the outlet opening balances the volume flow rate injected into the tank from the source plus the volume flow rate of the ambient air entrained by the emergent part of the fountain.

The presentation and discussion of the experimental results are postponed to Secs. III B and IV B for plume and fountain releases, respectively, in order to allow us to compare them with the theoretical models that will be presented thereafter.

III. SIMULTANEOUS FILLING AND EMPTYING WITH A PLUME

In this section we propose, as a first step, a theoretical model for the simultaneous filling and emptying of a box with a plume. This theoretical model incorporates the non-Boussinesq effects and the influence of the finite-size source. In a second step, the model will be validated against experimental data.

A. Theoretical model

As shown schematically in Fig. 3, we consider the simultaneous filling and emptying of a box with a turbulent plume. The height of the box is denoted by H and the surface of the ceiling is denoted by S. The source of the buoyant plume is defined by its density ρ_i, its radius b_i, and its volume flux $Q_i = \pi u_i b_i^2$. The fluid escapes from the box through a surface A at the ceiling with a mean velocity w. The thickness of the buoyant fluid layer that forms under the ceiling is denoted by z_a and its density, which is assumed to be homogeneous at any time, is denoted by ρ^*. By using this notation, the conservation equations for the mass and for the buoyancy of the buoyant layer read

$$\frac{d(S\rho^* z_a)}{dt} = Q_m - \rho^* wA, \tag{3}$$

$$\frac{d(g\eta^* S z_a)}{dt} = B_i - g\eta^* wA, \tag{4}$$

where $\eta^* = (\rho_a - \rho^*)/\rho_a$ is the buoyant-layer density deficit, $B_i = Q_i g(\rho_a - \rho_i)/\rho_a$ is the buoyancy flux at the source of the plume, and Q_m is the mass flow rate that feeds the fluid layer in the box. To evaluate the outlet velocity w, Bernoulli's theorem is applied between the buoyant-layer interface and the upstream of the outlet vent

$$\tfrac{1}{2}\rho^* w^2 = C_d^2 (\rho_a - \rho^*) g z_a, \tag{5}$$

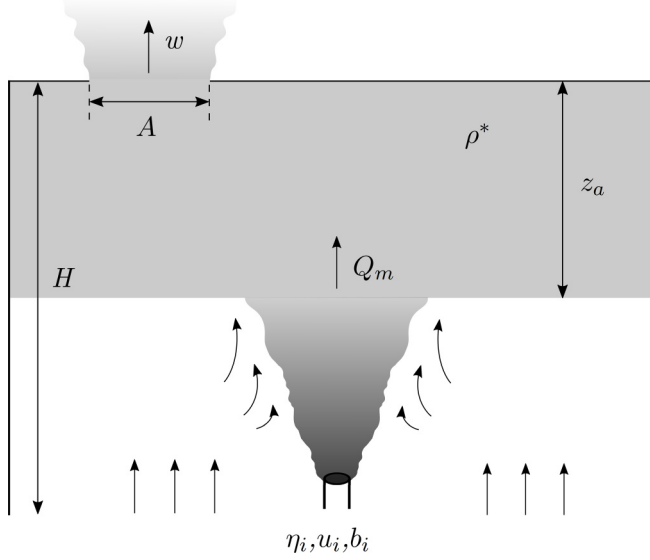where C_d is a coefficient coefficient [23].

FIG. 3. Schematic of the plume filling a box which is simultaneously emptied by an opening vent on the ceiling. Note that A corresponds to the vent area.

To accurately calculate Q_m, the plume model needs to consider the non-Boussinesq effects as well as the effects associated with the use of a finite-size source. To do this, the classical approach using the plume function Γ is used here. Indeed, following [5,12,27–32], in the general non-Boussinesq case, the plume characteristics, namely, the mean velocity u, the radius b, and the mean density deficit η, can be written as

$$u(z) = u_i \left(\frac{\Gamma_i}{\Gamma(z)} \right)^{1/2} \left(\frac{1 - \Gamma(z)}{1 - \Gamma_i} \right)^{1/10}, \tag{6}$$

$$b(z) = \sqrt{1 - \eta_i} b_i \left[1 + \frac{\eta_i}{1 - \eta_i} \left(\frac{\Gamma_i}{\Gamma(z)} \right)^{1/2} \left(\frac{1 - \Gamma(z)}{1 - \Gamma_i} \right)^{1/2} \right]^{1/2} \left(\frac{\Gamma(z)}{\Gamma_i} \right)^{1/2} \left(\frac{1 - \Gamma_i}{1 - \Gamma(z)} \right)^{3/10}, \tag{7}$$

$$\frac{\eta(z)}{1 - \eta(z)} = \frac{\eta_i}{1 - \eta_i} \left(\frac{\Gamma_i}{\Gamma(z)} \right)^{1/2} \left(\frac{1 - \Gamma(z)}{1 - \Gamma_i} \right)^{1/2}, \tag{8}$$

where the so-called plume function Γ is related to the vertical coordinate z via the differential equation

$$\frac{d\Gamma(z)}{dz} = \frac{4\alpha}{b_i \sqrt{1 - \eta_i}} \frac{\Gamma_i^{1/2}}{(1 - \Gamma_i)^{3/10}} \Gamma(z)^{1/2} [1 - \Gamma(z)]^{13/10}. \tag{9}$$

We recall that Γ_i is the source plume function. With these definitions, the mass flow rate Q_m can be evaluated as

$$Q_m = \rho_a Q_i (1 - \eta_i) \left(\frac{\Gamma}{\Gamma_i} \right)^{1/2} \left(\frac{1 - \Gamma_i}{1 - \Gamma} \right)^{1/2}. \tag{10}$$

At steady state (i.e., $t \to \infty$), the layer thickness as well as the density deficit in the layer can be evaluated by combining Eqs. (3)–(5) and (10). We obtain the set of
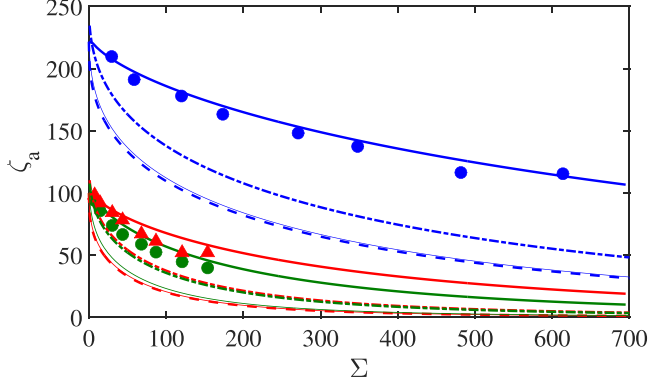
FIG. 4. Dimensionless thickness of the buoyant layer ζ_a as a function of the parameter Σ, for three different configurations. The thick solid lines correspond to the numerical solutions of Eqs. (12) and (13), the thin solid lines correspond to the numerical solutions of Eq. (14), the thick dashed lines corresponds to Eq. (15), and the thick dash-dotted lines correspond to Eq. (16). The symbols correspond to the experimental data: ●, configuration 1; ▲, configuration 2; and ■, configuration 3. Note that the entrainment coefficient α is set to 0.12.

equations

$$\eta^* = \frac{\eta_i}{\eta_i + (1 - \eta_i)\left(\frac{\Gamma_{ss}}{\Gamma_i}\right)^{1/2}\left(\frac{1-\Gamma_i}{1-\Gamma_{ss}}\right)^{1/2}}, \tag{11}$$

$$\zeta_a = \frac{(1 - \eta_i)^{5/2}}{\Gamma_i \Sigma^2}\left(\frac{\Gamma_{ss}}{\Gamma_i}\right)^{1/2}\left(\frac{1-\Gamma_i}{1-\Gamma_{ss}}\right)^{1/2}\left[\frac{\eta_i}{1-\eta_i} + \left(\frac{\Gamma_{ss}}{\Gamma_i}\right)^{1/2}\left(\frac{1-\Gamma_i}{1-\Gamma_{ss}}\right)^{1/2}\right]^2, \tag{12}$$

where $\zeta_a = z_a/b_i$ is the dimensionless thickness of the layer. The parameter Σ has been defined in the relation (2) and appears naturally in Eq. (12). This parameter takes into account the effects associated with the vent area. The parameter Γ_{ss} corresponds to the value of the function Γ at $z = z_a$. The value of Γ_{ss} can be evaluated from Eq. (9) as follows:

$$\zeta_a = \frac{H}{b_i} - \frac{\sqrt{1-\eta_i}}{4\alpha}\frac{|1-\Gamma_i|^{3/10}}{\Gamma_i^{1/2}}\int_{\Gamma_i}^{\Gamma_{ss}}\frac{d\gamma}{\gamma^{1/2}|1-\gamma|^{13/10}}. \tag{13}$$

By numerically solving the two coupled equations (12) and (13), the dimensionless layer thickness ζ_a can be evaluated and subsequently the density deficit η^*.

B. Comparison with experimental data

In this section the model developed for the simultaneous filling and emptying of a box with a plume is compared with experimental data. To do this, we focus on the thickness of the fluid layer under the ceiling. As a reminder, three different configurations are considered experimentally, corresponding to 24 experiments. For each configuration, the source conditions (Γ_i and η_i) and the box size (H/b_i) are kept constant, while the surface of the vent area (i.e., Σ) is varied.

The experimental data are plotted in Fig. 4 together with the theoretical predictions. Note that to compute the theoretical values, the coefficient C_d and the entrainment coefficient α are set to 0.7 and 0.12, respectively. It can be seen that, for fixed source conditions, the dimensionless layer thickness decreases as a function of the parameter Σ. Since the source plume conditions and the size of the box are fixed, the parameter Σ increases proportionally to the vent area. Thus, the larger the vent area is, the smaller the thickness of the buoyant layer will be. In particular, when $\Sigma = 0$, their is no opening and hence the buoyant-layer depth equals the tank depth, i.e., $\zeta_a = H/b_i$.

To evaluate the improvement brought by this model, the experimental and numerical results are compared with the simplified model obtained with the self-similar solutions of a point source plume. This model can be found in [9], where the layer thickness is expressed by the equation

$$\left[\left(\frac{H}{b_i} - \zeta_a\right)^{5/3} + \Theta\right]^2 \left(\frac{H}{b_i} - \zeta_a\right)^{5/3} = \left(\frac{5}{6\alpha}\right)^5 \Sigma^2 \zeta_a, \tag{14}$$

where

$$c = \frac{1}{3}\left(\frac{25}{6\pi\alpha^2}\right)^{2/3}, \quad \Theta = \frac{cB^{2/3}}{gH^{5/3}}.$$

Note that the non-Boussinesq effects are taken into account through the parameter Θ. By setting $\Theta = 0$ in (14), the classical Boussinesq case (see [8,26]) is then recovered as

$$\left[\frac{H}{b_i} - \zeta_a\right]^5 = \left(\frac{5}{6\alpha}\right)^5 \Sigma^2 \zeta_a. \tag{15}$$

This relation shows that in the Boussinesq case and for point source conditions, the layer thickness is simply obtained through the geometrical parameters H/b_i and Σ. Both Boussinesq and non-Boussinesq relations are plotted in Fig. 4. As can be seen, the theoretical predictions of the simplified models follow the same behavior as the experimental data. However, they predict much thinner thickness than what is actually seen. This is true even with the simplified model taking into account non-Boussinesq effects. To improve those models, Woods *et al.* [25] proposed a model that accounts for the effect associated with the lower opening as well as for the virtual origin correction. They obtained an implicit equation which reads

$$\left(\frac{\Sigma^2 + \Sigma'^2}{\Sigma'^2}\right)\left(\frac{H}{b_i} - \zeta_a + \zeta_v\right)^5 - 2\frac{\Sigma^2}{\Sigma'^2}\zeta_v^{5/3}\left(\frac{H}{b_i} - \zeta_a + \zeta_v\right)^{10/3} + \zeta_v^{10/3}\frac{\Sigma^2}{\Sigma'^2}\left(\frac{H}{b_i} - \zeta_a + \zeta_v\right)^{5/3}$$

$$= \left(\frac{5}{6\alpha}\right)^5 \Sigma^2 \zeta_a, \tag{16}$$

where ζ_v is the dimensionless virtual origin corrected by the source volume flux defined as

$$\zeta_v = \left(\frac{5}{6\alpha}\right)^{3/5}\left(\frac{10}{9\pi^2\alpha}\right)^{1/5}\frac{Q_i^{3/5}}{b_i B_i^{1/5}}$$

and the parameter Σ' as

$$\Sigma' = \frac{4\sqrt{\alpha}C_d S}{\sqrt{5}\pi b_i^2},$$

where S is the surface of the lower boundary, which is completely open. As can be seen, when $\Sigma' \to \infty$, Eq. (16) tends to that of a plume issuing from a point source, i.e., Eq. (15). It can be observed in Fig. 4 that this model allows us to improve the theoretical predictions as compared to those using the self-similar solutions of the plume variables. This shows that the better the primary variables are modeled near the source, the better the predictions are. Obviously, by using the Γ function, which actually turns out to be equivalent to solving numerically the Morton-Taylor-Turner equations, the agreement is even better.

IV. SIMULTANEOUS FILLING AND EMPTYING WITH A FOUNTAIN

This section is devoted to the fountain problem. When the steady state is reached, there are two possibilities: Either the fountain is fully submerged by the buoyant layer or the fountain is only partially submerged by the buoyant layer. In the first case, there is no air entrainment at the bottom
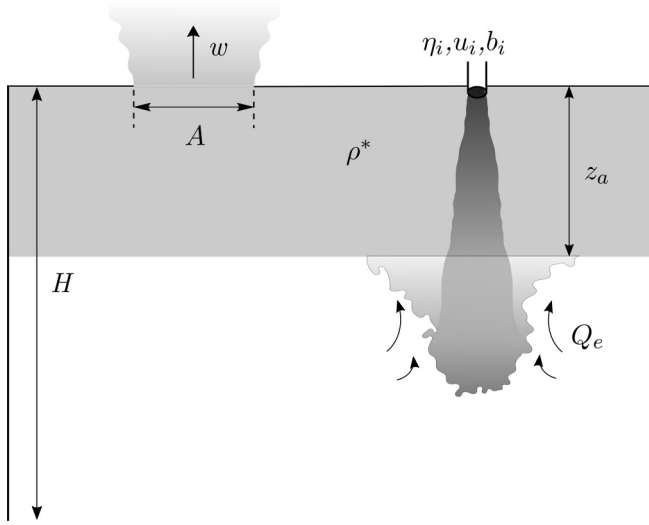
FIG. 5. Schematic of the fountain filling a box which is simultaneously emptied by an opening vent on the ceiling. Note that A corresponds to the vent area.

of the cylinder tank (which is fully open to the atmosphere). As a result, the volume flow rate at the outlet vent must be equal to that injected into the tank from the source. The second case is more interesting. When the fountain is only partially submerged, the volume flow rate at the outlet vent balances the volume flow rate discharged at the source plus the volume flow rate of the ambient air entrained by the fountain which comes from the bottom of the cylinder tank. The model developed in this section will analyze these two situations.

A. Theoretical model

Similarly to the plume problem, the fountain source volume flux is denoted by Q_i and its density is denoted by ρ_i (see Fig. 5). The conservation equations for the mass and for the buoyancy of the buoyant layer are however slightly different. They are written as

$$\frac{d(S\rho^* z_a)}{dt} = \rho_i Q_i + \rho_a Q_e - \rho^* wA, \tag{17}$$

$$\frac{d(g\eta^* S z_a)}{dt} = B_i - g\eta^* wA, \tag{18}$$

where Q_e is the volume flux of ambient fluid entrained by the fountain. Concerning the outlet velocity w, it is identical to the expression [5] given in the plume problem. Note that the density ρ^* is assumed to be uniform in the buoyant fluid layer.

To complete the model, a closure model is still required for the volume flux entrained by the fountain (i.e., Q_e). Here we first focus on the situation where the fountain is not submerged by the buoyant layer. In the case of filling a box with Boussinesq fountains, Baines *et al.* [14] showed that the entrained volume is proportional to the emergent part of the fountain, i.e., proportional to $z_f - z_a$. In the present case of non-Boussinesq fountains, we propose the expression

$$Q_e = \beta_{nb}\left(\frac{\rho_i}{\rho_a}\right)^{1/2}\frac{Q_i}{b_i}(z_f - z_a), \tag{19}$$

where β_{nb} is a constant that plays the role of an entrainment coefficient for the turbulent fountains. In comparison with the relation proposed by Baines *et al.* [14], this constant of proportionality involved

in their expression has been replaced by $\beta_{nb}(\rho_i/\rho_a)^{1/2}$ in order to take into account the effects of density difference [33].

Having now established an entrainment model for the fountain, we are able to evaluate the simultaneous filling and emptying process at steady state. Using Eqs. (19) and (5) in (17) and (18), at the steady state, we are led to the set of equations

$$\frac{\Sigma(1 - \eta_i)^{1/4}}{\eta_i^{1/2}\Gamma_i^{1/2}}\sqrt{(1 - \eta^*)\eta^*\zeta_a} = (1 - \eta_i)^{1/2} + \beta_{nb}(\zeta_f - \zeta_a), \tag{20}$$

$$\left(\frac{\eta^*}{\eta_i}\right)^{3/2}\left(\frac{1 - \eta_i}{1 - \eta^*}\right)^{1/2}\frac{(1 - \eta_i)^{1/4}\Sigma\zeta_a^{1/2}}{\Gamma_i^{1/2}} = 1, \tag{21}$$

where $\zeta_f = z_f/b_i$ is dimensionless fountain height. By dividing Eq. (20) by (21), we obtain, for the density deficit of the buoyant layer, the expression

$$\eta^* = \frac{\eta_i}{1 + \beta_{nb}(1 - \eta_i)^{1/2}(\zeta_f - \zeta_a)}. \tag{22}$$

By combining the relations (21) and (22), after some algebra, the following equation is obtained:

$$(\zeta_f - \zeta_a)^3 + \frac{3 - \eta_i}{\beta_{nb}(1 - \eta_i)^{1/2}}(\zeta_f - \zeta_a)^2 + \left(\frac{3 - 2\eta_i}{\beta_{nb}^2(1 - \eta_i)} + \frac{\Gamma_i\Sigma^2}{(1 - \eta_i)\beta_{nb}^3}\right)(\zeta_f - \zeta_a)$$

$$-\frac{\Gamma_i\Sigma^2}{(1 - \eta_i)\beta_{nb}^3}\zeta_f + \frac{1}{(1 - \eta_i)^{1/2}\beta_{nb}^3} = 0. \tag{23}$$

This cubic equation admits three roots. Two of these roots are complex and the third one is real and positive. It corresponds to the stabilized buoyant-layer depth.

In the case where the fountain is completely submerged, the entrained volume flux is identically null (i.e., $Q_e = 0$). Thus, by using the previous notation, we obtain

$$\eta = \eta_i, \tag{24}$$

$$\zeta_a = \frac{\sqrt{1 - \eta_i}}{\Gamma_i\Sigma^2}. \tag{25}$$

From these relations, it is easy to seen that if

$$\Sigma > \frac{(1 - \eta_i)^{1/4}}{(\Gamma_i\zeta_a)^{1/2}}, \tag{26}$$

then the fountain is not fully submerged by the buoyant layer. Consequently, in that case, Eq. (23) still holds for the evaluation of the buoyant-layer depth.

B. Comparison with experimental data

The comparison between the theory and the experiments essentially focuses on the stabilized buoyant-layer depth. Indeed, its value is evaluated for each experiment and compared to the theoretical value derived from Eq. (23). However, before proceeding with this comparison, estimations of the free parameters β_{nb} and ζ_f are needed.

Concerning the value of ζ_f, it is evaluated directly from experimental data. Figure 6 shows the fountain height measured at the steady state as a function of the length scale $\mathcal{L}_b$. It can be seen that it is well approximated by

$$z_f \approx 1.8\mathcal{L}_b, \tag{27}$$

where the length scale $\mathcal{L}_b$ is defined as $\mathcal{L}_b = (M_i/\rho_i)^{3/4}/[Bi(\rho_a/\rho_i)]^{1/2}$ (see [20,35]) and the momentum flux as $M_i = \pi\rho_i b_i^2 u_i^2$. This length scale was originally introduced by Turner [6], who
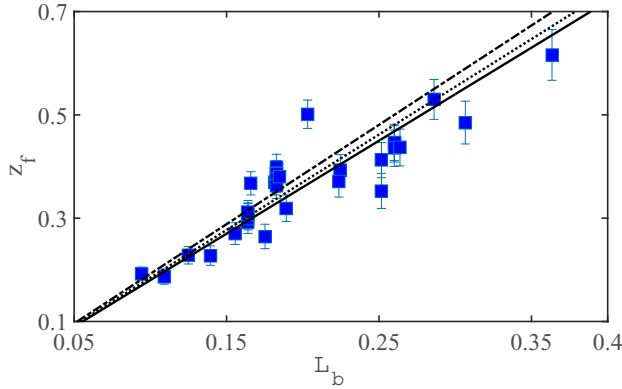
FIG. 6. Plot of the fountain height as a function of the length scale $\mathcal{L}_b$. The blue squares correspond to the experimental points, the black solid line corresponds to $z_f \approx 1.8\mathcal{L}_b$, the black dotted line corresponds to $z_f \approx 1.84\mathcal{L}_b$ given by [6,34], and the black dashed line corresponds to $z_f \approx 1.92\mathcal{L}_b$ given by [20]. The bars correspond to the amplitude of oscillation of the fountain height set to $0.14\mathcal{L}_b$ as suggested in [20].

found $z_f \approx 1.84\mathcal{L}_b$ for a forced fountain in the Boussinesq case. Mehaddi *et al.* [20] extended this result for the case of non-Boussinesq fountains and found experimentally a coefficient of proportionality of 1.92. This result was confirmed numerically by Vaux *et al.* [35] with a slightly different coefficient of proportionality of 1.8.

Note that the fountain height fluctuates naturally around a mean value. As shown in [36] for a Boussinesq fountain and in [20] for non-Boussinesq fountains, the amplitude of fluctuations of the fountain height is proportional to the jet length, meaning that $\delta z \propto \mathcal{L}_b$. In Fig. 6 these oscillations have been incorporated in the form of bars with an amplitude $\delta z \approx 0.14\mathcal{L}_b$ (see [20]).

For the coefficient β_{nb}, in the Boussinesq case (i.e., $\rho_i/\rho_a \to 1$), Baines *et al.* [14] set the value of β_{nb} equal to 0.25, while Burridge and Hunt [37] showed that a good value for this coefficient, in their case of forced Boussinesq fountains in unbounded environment, lies between 0.29 and 0.32. Thus, it can be expected that a value of $\beta_{nb} \approx 0.3$ may be used for our problem. However, the simplification, which consists in considering that the majority of the entrained fluid comes from the fountain lateral edges, may be insufficient. Indeed, a part of the entrained fluid may also come from the fountain top. Accordingly to account for a part of this effect, the value of β_{nb} may be adjusted to fit experimental data. As a result, in the present investigation, the value of this coefficient is varied systematically to minimize the difference between experiments and theory. The coefficient of determination R^2 around the one-to-one line is evaluated for $\beta_{nb} = (0.25, 0.30, 0.35, 0.40, 0.45)$; we find $R^2 = (0.68, 0.79, 0.84, 0.84, 0.83)$, respectively. Thus, in the following, the value $\beta_{nb} = 0.35$ is chosen.

In Fig. 7(a) the thickness z_a is plotted as a function of the jet length $\mathcal{L}_b$ for a fixed value of the outlet surface and with different values of the density ratio η_i. We obtain that the thickness of the fluid layer varies linearly as a function of $\mathcal{L}_b$. In this figure the theory is represented in the form of two curves for two limiting values of η_i, namely, $\eta_i = 0.2$ and 0.9. We notice that the theory reproduces in a satisfactory way the variation of the thickness z_a. We also notice that the density deficit has a negligible effect on this thickness. In Fig. 7(b) we have also plotted the variation of the thickness for two different vent areas, namely, $\Sigma = 14.1$ and 31.8. Here again it can be observed that the model reproduces satisfactorily the behavior of the thickness as a function of $\mathcal{L}_b$. To reinforce these results we have fixed the value of jet length $\mathcal{L}_b$ or in other terms (Γ_i and η_i) while varying the sizes of the outlets. Therefore, as can be seen in Fig. 8, we observe the same behavior as the plume case, namely, the decrease of the layer thickness as a function of the parameter Σ, and this behavior is satisfactorily reproduced by the present model.
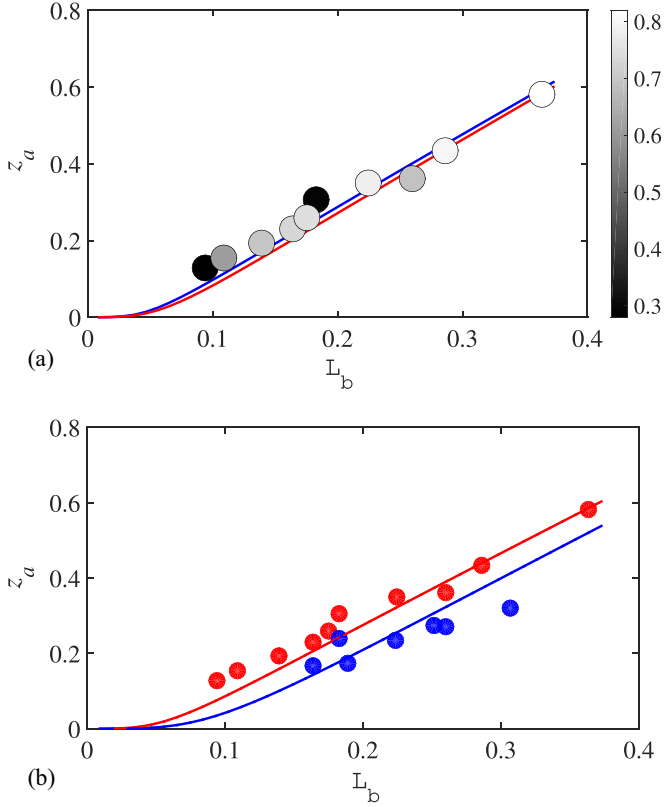
FIG. 7. (a) Variation of z_a as a function of $\mathcal{L}_b$ for a fixed value of $\Sigma = 14.1$. The experimental data are shaded according to the density deficit η_i; the blue line corresponds to the numerical solution of (23) with $\eta_i = 0.2$ and the red line corresponds to $\eta_i = 0.9$. (b) Variation of z_a as a function of $\mathcal{L}_b$ for two different values of Σ. The colored circles correspond to experimental data and the lines correspond to the theoretical predictions. Red corresponds to $\Sigma = 14.1$ and blue corresponds to $\Sigma = 31.8$.
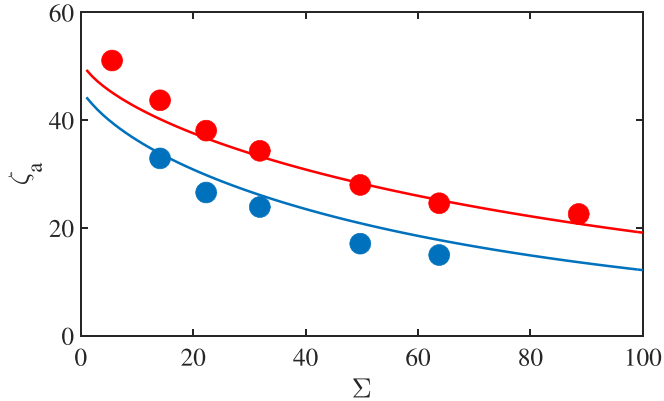

FIG. 8. Variation of ζ_a as a function Σ for two different values of Γ_i: $\Gamma_i = 0.0087$ (blue) and $\Gamma_i = 0.0114$ (red).
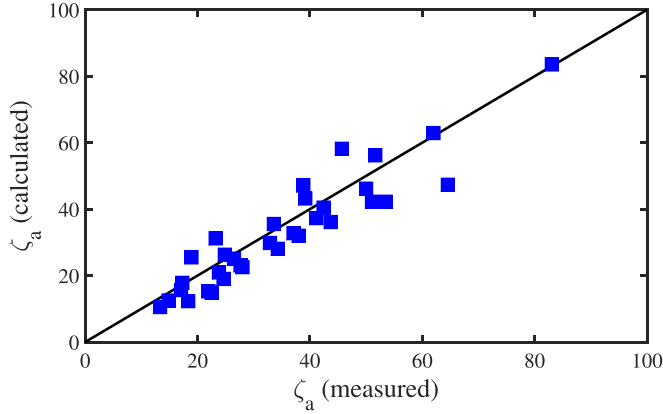
FIG. 9. Comparison between the experimental data and the numerical solution of (23).

Finally, Fig. 9 shows the comparison between all the experimental points and the theoretical results. As it can be seen, fairly good agreement is achieved.
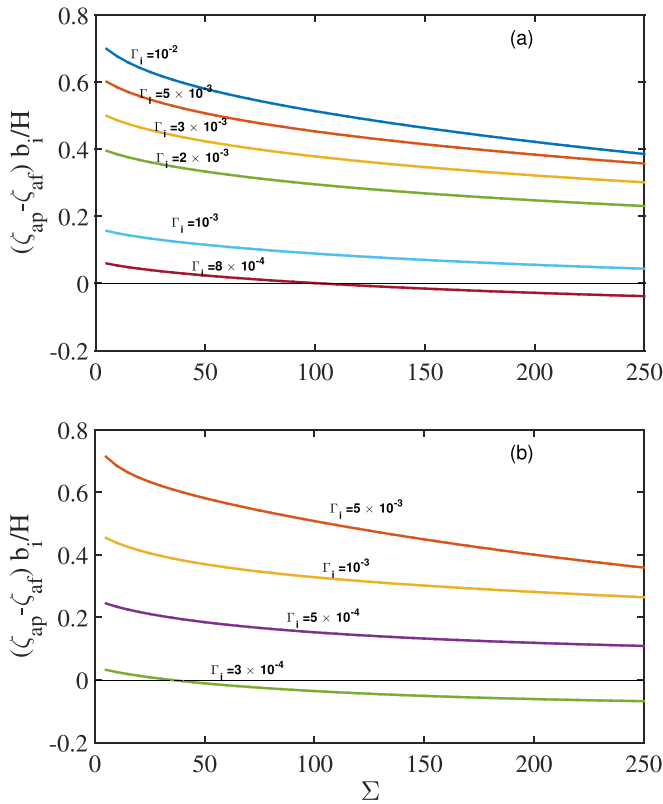

FIG. 10. Difference $(\zeta_{a_p} - \zeta_{a_f})b_i/H$ as a function of Σ for different values of Γ_i, $H/b_i = 200$, and (a) $\eta_i = 0.05$ and (b) $\eta_i = 0.85$. The thin solid lines correspond to $\zeta_{a_p} - \zeta_{a_f} = 0$.
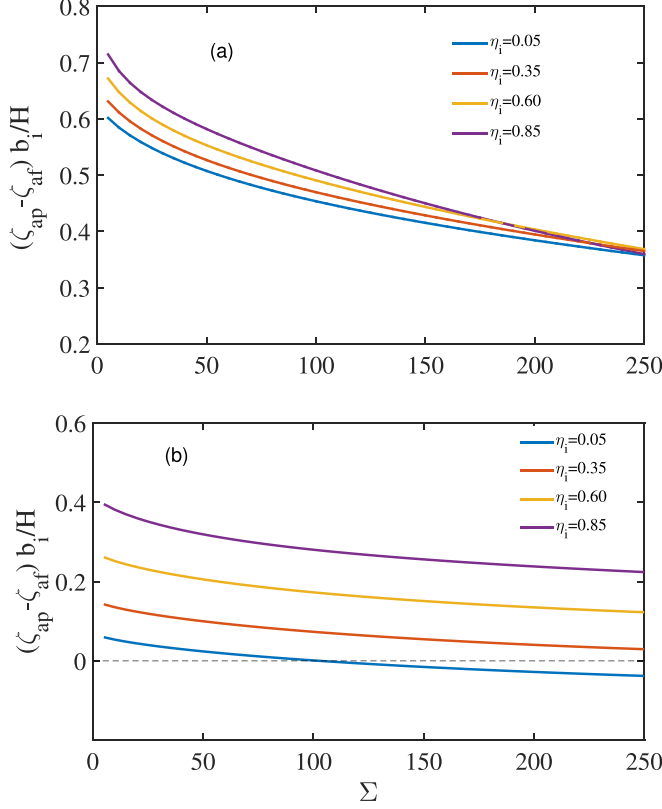
FIG. 11. Difference $(\zeta_{a_p} - \zeta_{a_f})b_i/H$ as a function of Σ for different values of η_i, $H/b_i = 200$, and (a) $\Gamma_i = 5 \times 10^{-3}$ and (b) $\Gamma_i = 8 \times 10^{-4}$. The thin dashed line in (b) corresponds to $\zeta_{a_p} - \zeta_{a_f} = 0$.

V. COMPARISON BETWEEN PLUME AND FOUNTAIN CONFIGURATIONS

So far we have established two theoretical models for the simultaneous filling and emptying of an enclosure. As a reminder, the configurations considered are the release of a light fluid under the form of a turbulent plume or under the form of a turbulent fountain. The question that can now be asked is which configuration (fountain or plume) results in a larger fluid layer and in a lower density deficit. Alternatively, for given source conditions and enclosure size, does a plume entrain more efficiently its surrounding than a fountain? To answer this question let us note that from the two models, the following functional relations can be inferred:

$$\zeta_{a_f}, \quad \eta_f^* = f(\Gamma_i, \Sigma, \eta_i), \quad \zeta_f < \frac{H}{b_i}, \tag{28}$$

$$\zeta_{a_p}, \quad \eta_p^* = f\left(\Gamma_i, \Sigma, \eta_i, \frac{H}{b_i}\right). \tag{29}$$

Here ζ_{a_f}, ζ_{a_p}, η_f^*, and η_p^* are the layer depth resulting from the fountain configuration, the layer depth resulting from the plume, the density in the fountain configuration, and the density in the plume configuration, respectively. It is seen in relation (28) that the height of the box is an implicit parameter which limits the height of the fountain ζ_f.

We first discuss the plume and fountain configurations in terms of the layer depth. To evaluate which configuration gives rise to the largest layer, we plot in Figs. 10 and 11 the difference $(\zeta_{a_p} - \zeta_{a_f})b_i/H$. If the resulting layer from a plume release is larger than the layer resulting from a
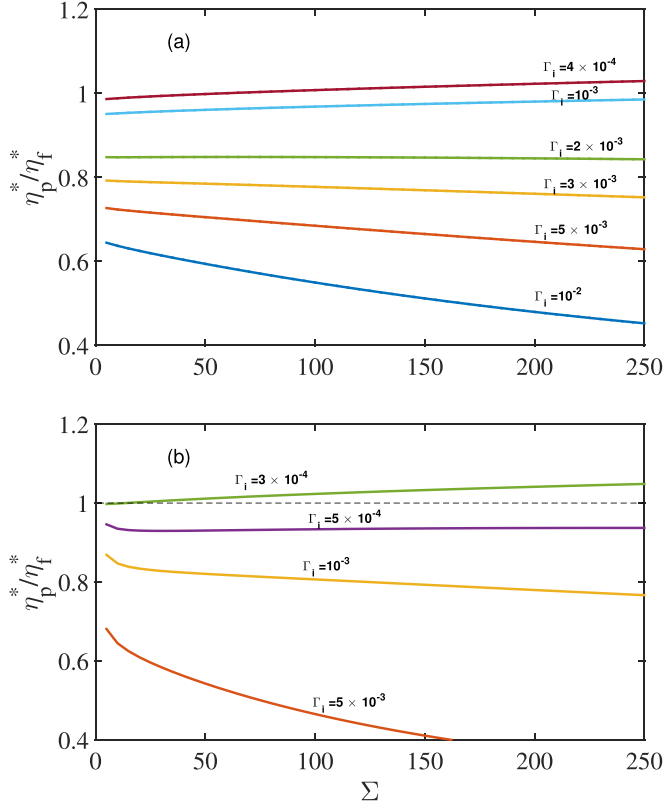
FIG. 12. Ratio η_p^*/η_f^* as a function of Σ for different values of Γ_i, $H/b_i = 200$, and a source density deficit of (a) $\eta_i = 0.05$ and (b) $\eta_i = 0.85$. The thin dashed line in (b) corresponds to $\eta_p^*/\eta_f^* = 1$.

fountain release, then the ratio $(\zeta_{a_p} - \zeta_{a_f})b_i/H$ will be positively valued. In Figs. 10(a) and 10(b), $(\zeta_{a_p} - \zeta_{a_f})b_i/H$ is plotted as a function of Σ for fixed η_i and Γ_i. In that case, an increase of Σ corresponds to the increase of the vent area A. Let us first note that for a fixed Γ_i, the difference $(\zeta_{a_p} - \zeta_{a_f})b_i/H$ decreases according to the parameter Σ. Indeed, an increase in the value of Σ induces, for similar injection conditions, a decrease in the thickness of the fluid layer in both configurations. However, in view of Fig. 8, it appears that the thickness of the fluid layer decreases more for the plume configuration than for the fountain configuration. Moreover, it can also be seen that the value of $(\zeta_{a_p} - \zeta_{a_f})b_i/H$ approaches zero as Γ_i decreases. In particular, it is observed that for large values of Σ, the layer resulting from the fountain becomes bigger than that of the plume. However, it can also be seen that for the majority of situations, the plume configuration seems to be more efficient. In Figs. 11(a) and 11(b) the influence of the density deficit is depicted for two different values of the parameter Γ_i. It can be seen that the efficiency of the plume configuration diminishes as the density deficit η_i increases. This fact can be explained by the strong dependence of the plume entrainment coefficient on the density deficit.

In Figs. 12 and 13 the ratio η_p^*/η_f^* is plotted as a function of the parameter Σ. If $\eta_p^*/\eta_f^* < 1$ corresponding to $\Delta\rho_p^* < \Delta\rho_f^*$, the plume configuration mixes more efficiently with the ambient fluid, while in the opposite case ($\eta_p^*/\eta_f^* > 1$) it is the fountain that mixes better. In Figs. 12(a) and 12(b) the ratio η_p^*/η_f^* is plotted for a fixed η_i and different values of Γ_i. It can be seen that similarly to the layer depth, the ratio η_p^*/η_f^* is lower than 1, which confirms that the plume configuration is more efficient in the majority of the tested situations in terms of mixing. However, below a certain value of Γ_i, the fountain configuration produces a layer with lower density than the plume case.
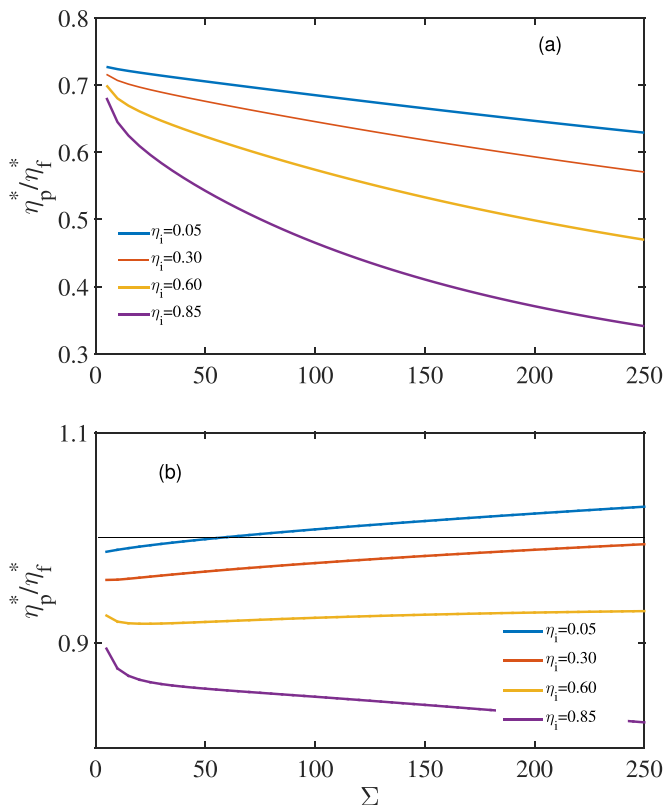
FIG. 13. Ratio η_p^*/η_f^* as a function of Σ for different values of η_i, $H/b_i = 200$, and (a) $\Gamma_i = 5 \times 10^{-3}$ and (b) $\Gamma_i = 8 \times 10^{-4}$. The thin solid line in (b) corresponds to $\eta_p^*/\eta_f^* = 1$.

In Figs. 13(a) and 13(b) the effect of the source density deficit is evaluated by fixing the parameter Γ_i and varying η_i. It can be seen that the non-Boussinesq effects (larger values of η_i) do not change the general trend of the ratio η_p^*/η_f^* as a function of Σ for $\Gamma_i = 5 \times 10^{-3}$. In that case, the plume always dominates because the fountain height is not large enough to mix its surrounding.

VI. CONCLUSION

In this paper we have investigated theoretically and experimentally the simultaneous filling and emptying of a box in the non-Boussinesq case. Two configurations have been considered, namely, the configuration where a light fluid was released from the bottom (plume) and the case where a light fluid was released from above (fountain). In both configurations, the compartment contains a vent area at the ceiling. To compare these configurations, a model for the plume filling box was first established. The model is based on the plume theory expressed with the Γ function and in the non-Boussinesq general case. This configuration allowed us to take into account the density effects and also the effects associated with the finite-size source. Experiments were conducted with an air-helium setup for the plume filling box model. The comparison between the experiments and the model showed good agreement. In addition, a model for the fountain filling box model was also established. This model is based on a formulation of the fountain entrainment that accounts for the non-Boussinesq effects. Here again an experimental campaign was undertaken. The experimental data were compared to the theory and fairly well agreement was observed.

Finally, these two models were compared in the case where the fountain and the plume have the same source conditions and fixed box geometrical characteristics (the box height and the vent area). This comparison has shown that the plume configuration produced, in most cases, a thicker layer of fluid under the ceiling and therefore an average density lower than that resulting from a fountain discharge. As the jet length $\mathcal{L}_b$ increases, the gap between the fountain and plume configurations decreases. This observation simply reflects the proportional relationship between the height of the fountain and the entrainment rate. Thus, beyond a certain value of the jet length $\mathcal{L}_b$, the fountain configuration becomes better in terms of its ability to produce a wider layer and better mixed with its environment. This final result is of importance in applications where a choice may have to be made between an upward or a downward discharge.

[1] S. Nabi and M. R. Flynn, The hydraulics of exchange flow between adjacent confined building zones, Build. Environ. **59**, 76 (2013).

[2] A. E. Germeles, Forced plumes and mixing of liquids in tanks, J. Fluid Mech. **71**, 601 (1975).

[3] J. S. Turner and I. H. Campbell, Convection and mixing in magma chambers, Earth-Sci. Rev. **23**, 255 (1986).

[4] L. J. Bloomfield and R. C. Kerr, Turbulent fountains in a confined stratified environment, J. Fluid Mech. **389**, 27 (1999).

[5] B. R. Morton, Forced plumes, J. Fluid Mech. **5**, 151 (1959).

[6] J. S. Turner, Jets and plumes with negative or reversing buoyancy, J. Fluid Mech. **26**, 779 (1966).

[7] R. Mehaddi, S. Vaux, F. Candelier, and O. Vauquelin, On the modelling of steady turbulent fountains, Environ. Fluid Mech. **15**, 1115 (2015).

[8] P. F. Linden, G. F. Lane-Serff, and D. A. Smeed, Emptying filling boxes: The fluid mechanics of natural ventilation, J. Fluid Mech. **212**, 309 (1990).

[9] O. Vauquelin, Oscillatory behaviour in an emptying–filling box, J. Fluid Mech. **781**, 712 (2015).

[10] B. R. Morton, G. I. Taylor, and J. S. Turner, Turbulent gravitational convection from maintained and instantaneous sources, Proc. R. Soc. London Ser. A **234**, 1 (1956).

[11] G. R. Hunt and N. G. Kaye, Virtual origin correction for lazy turbulent plumes, J. Fluid Mech. **435**, 377 (2001).

[12] G. Michaux and O. Vauquelin, Solutions for turbulent buoyant plumes rising from circular sources, Phys. Fluids **20**, 066601 (2008).

[13] F. Candelier and O. Vauquelin, Matched asymptotic solutions for turbulent plumes, J. Fluid Mech. **699**, 489 (2012).

[14] W. D. Baines, J. S. Turner, and I. H. Campbell, Turbulent fountains in an open chamber, J. Fluid Mech. **212**, 557 (1990).

[15] D. T. Bolster and P. F. Linden, Contaminants in ventilated filling boxes, J. Fluid Mech. **591**, 97 (2007).

[16] N. B. Kaye and G. R. Hunt, Smoke filling time for a room due to a small fire: The effect of ceiling height to floor width aspect ratio, Fire Safety J. **42**, 329 (2007).

[17] S. H. Harrak, R. Mehaddi, P. Boulet, E. M. Koutaiba, G. Giovannelli, and S. Becker, Virtual origin correction for a fire plume in a room under displacement ventilation regime, Int. J. Therm. Sci. **136**, 243 (2019).

[18] S. Haouari-Harrak, R. Mehaddi, P. Boulet, and E. M. Koutaiba, Evaluation of the room smoke filling time for fire plumes: Influence of the room geometry, Fire Mater. **44**, 793 (2020).

[19] Q. A. Liu and P. F. Linden, The fluid dynamics of an underfloor air distribution system, J. Fluid Mech. **554**, 323 (2006).

[20] R. Mehaddi, O. Vauquelin, and F. Candelier, Experimental non-Boussinesq fountains, J. Fluid Mech. **784** (2015).

[21] A. Lamorlette, R. Mehaddi, and O. Vauquelin, Unstable modes of laminar round fountains on inclined wall, C. R. Mec. **339**, 250 (2011).

[22] A. J. Ward-Smith, *Internal Fluid Flow: The Fluid Dynamics of Flow in Pipes and Ducts* (Oxford University Press, New York, 1980).

[23] O. Vauquelin, E. M. Koutaiba, E. Blanchard, and P. Fromy, The discharge plume parameter γ_d and its implications for an emptying-filling box, J. Fluid Mech. **817**, 171 (2017).

[24] G. R. Hunt and J. M. Holford, *Proceedings of the 21st AIVC Conference on Innovations in Ventilation Technology, Hague, 2000* (AIVC, Sint-Stevens-Woluwe, 2000).

[25] A. W. Woods, C. Caulfield, and J. C. Phillips, Blocked natural ventilation: The effect of a source mass flux, J. Fluid Mech. **495**, 119 (2003).

[26] P. F. Linden, The fluid mechanics of natural ventilation, Annu. Rev. Fluid Mech. **31**, 201 (1999).

[27] G. R. Hunt and T. S. van den Bremer, Classical plume theory: 1937–2010 and beyond, IMA J. Appl. Math. **76**, 424 (2011).

[28] P. Carlotti and G. R. Hunt, Analytical solutions for turbulent non-Boussinesq plumes, J. Fluid Mech. **538**, 343 (2005).

[29] T. S. van den Bremer and G. R. Hunt, Universal solutions for Boussinesq and non-Boussinesq plumes, J. Fluid Mech. **644**, 165 (2010).

[30] G. G. Rooney and P. F. Linden, Similarity considerations for non-Boussinesq plumes in an unstratified environment, J. Fluid Mech. **318**, 237 (1996).

[31] G. R. Hunt and N. B. Kaye, Lazy plumes, J. Fluid Mech. **533**, 329 (2005).

[32] T. K. Fanneløp and D. M. Webber, On buoyant plumes rising from area sources in a calm environment, J. Fluid Mech. **497**, 319 (2003).

[33] F. P. Ricou and D. B. Spalding, Measurements of entrainment by axisymmetrical turbulent jets, J. Fluid Mech. **11**, 21 (1961).

[34] H. C. Burridge and G. R. Hunt, The rise heights of low-and high-Froude-number turbulent axisymmetric fountains, J. Fluid Mech. **691**, 392 (2012).

[35] S. Vaux, R. Mehaddi, O. Vauquelin, and F. Candelier, Upward versus downward non-Boussinesq turbulent fountains, J. Fluid Mech. **867**, 374 (2019).

[36] H. C. Burridge and G. R. Hunt, The rhythm of fountains: The length and time scales of rise height fluctuations at low and high Froude numbers, J. Fluid Mech. **728**, 91 (2013).

[37] H. C. Burridge and G. R. Hunt, Entrainment by turbulent fountains, J. Fluid Mech. **790**, 407 (2016).